

A microfluidic system with optical laser tweezers to study mechanotransduction and focal adhesion recruitment†

Peyman Honarmandi, Hyungsuk Lee, Matthew J. Lang and Roger D. Kamm*

Received 7th October 2010, Accepted 17th November 2010

DOI: 10.1039/c0lc00487a

We present a new method to locally apply mechanical tensile and compressive force on single cells based on integration of a microfluidic device with an optical laser tweezers. This system can locate a single cell within customized wells exposing a square-like membrane segment to a functionalized bead. Beads are coated with extracellular matrix (ECM) proteins of interest (*e.g.* fibronectin) to activate specific membrane receptors (*e.g.* integrins). The functionalized beads are trapped and manipulated by optical tweezers to apply mechanical load on the ECM-integrin-cytoskeleton linkage. Activation of the receptor is visualized by accumulation of expressed fluorescent proteins. This platform facilitates isolation of single cells and excitation by tensile/compressive forces applied directly to the focal adhesion *via* specific membrane receptors. Protein assembly or recruitment in a focal adhesion can then be monitored and identified using fluorescent imaging. This platform is used to study the recruitment of vinculin upon the application of external tensile force to single endothelial cells. Vinculin appears to be recruited above the forced bead as an elliptical cloud, centered $2.1 \pm 0.5 \mu\text{m}$ from the $2 \mu\text{m}$ bead center. The mechanical stiffness of the membrane patch inferred from this measurement is $42.9 \pm 6.4 \text{ pN } \mu\text{m}^{-1}$ for a $5 \mu\text{m} \times 5 \mu\text{m}$ membrane segment. This method provides a foundation for further studies of mechanotransduction and tensile stiffness of single cells.

Introduction

Cells exert forces on adjacent cells or the extracellular matrix (ECM) *via* various transmembrane adhesion proteins. These intercellular and ECM interactions play a crucial role in regulating cellular functions such as migration,¹ differentiation,² proliferation,³ and apoptosis.⁴ Cell–ECM interactions mostly occur through the heterodimeric interactions between matrix molecules and various members of the integrin family. As a pathway for force transmission to the cytoskeleton, integrins play an important role in mechanotransduction through focal adhesion (FA) proteins that serve to link the integrin cytoplasmic domains to the actin filaments forming an adhesion complex. Talin and vinculin are among the numerous FA proteins that link the cytoplasmic domains of integrin subunits to F-actin filaments.^{5–7} Talin has a spherical head with an elongated rod domain that provides an essential structural link between integrins and the actin cytoskeleton. The head domain of talin has a binding site for β -integrin⁸ as well as for F-actin,⁹ while the rod domain contains an additional binding site for β -integrin,^{10,11} at least two binding sites for F-actin¹² and 11 binding sites for vinculin.¹³ Vinculin is a cytoplasmic protein that consists of a globular head and a rod-like tail domain, which contains binding sites for many other cytoplasmic proteins including talin and F-actin.^{14–16} The vinculin head is known to bind to talin,¹⁷

whereas the tail domain is known to bind F-actin.¹⁸ Given these known binding characteristics, cell–ECM initial contacts may consist of fibronectin, integrin, talin, and F-actin linkages as shown schematically in Fig. 1.

One important mechanism by which cells regulate integrin function is through rapid, reversible control of integrin affinity for extracellular ligands, so-called integrin activation.¹⁹ It has been shown that integrins can participate both in inside-out and outside-in signaling. For example, integrin activation is known to be mediated by talin binding to the intracellular domain.²⁰ Besides, force applications to the extracellular domain is known to stimulate activation of intracellular proteins, which then alters their interactions with other cytoplasmic proteins.²¹ In particular, after integrin activation, forces transmitted from integrin to talin are capable of activating talin, leading to vinculin recruitment. This mechanism has been studied computationally providing support for the hypothesis that force acting on talin can cause a conformational change that exposes the cryptic vinculin-binding sites.^{22–24} However, solid experimental evidence is still needed to assess this hypothesis in the cells under the presence of tension.²⁵

In the last decade, several experiments have investigated the importance of mechanosensing and the assembly of focal complexes at adhesion sites under the application of mechanical force with various ECM proteins.^{26–29} These studies demonstrated that mechanical forces are required for the initiation and formation of focal complexes through a process termed mechanotransduction. Detailed studies are difficult, however, due to the challenges of applying precise levels of tensile force to the cell under closely regulated conditions. Although more than 40 proteins are known to be present in FA domains, it is not known

Massachusetts Institute of Technology (MIT), Department of Biological Engineering, Massachusetts Institute of Technology, Cambridge, MA, 02139, USA. E-mail: rdkamm@mit.edu; Fax: +1(617) 253-6236; Tel: +1(617) 253 5330

† Electronic supplementary information (ESI) available: Table 2; Movie S0, S1 and S2. See DOI: 10.1039/c0lc00487a

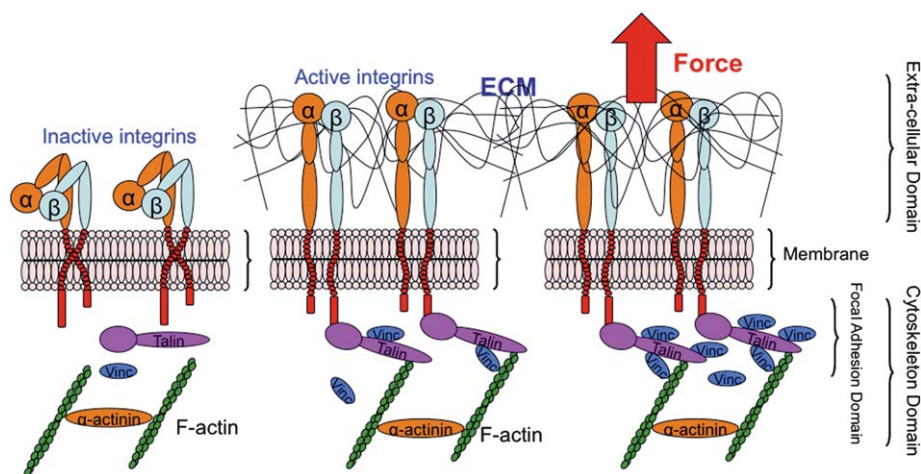


Fig. 1 Schematic representation of activated integrin and formation of ECM-integrin-cytoskeleton linkages in focal adhesion site upon application of an external tensile load.

how many of these are implicated in mechanotransduction. New methods are therefore needed to systematically examine these and their localization to a FA, or other adhesion complexes, under the application of force.

In this research, a microfluidic device and optical laser tweezers are used to apply mechanical stimuli to cells. Using microfluidics provides convenient means of introducing and positioning cells under controlled and physiological conditions. In this particular instance, a microfluidic device was designed to confine the cells and to expose a portion of the cell membrane to a bead functionalized with an integrin-binding protein, *e.g.* fibronectin, to emulate ECM-integrin-cytoskeleton linkages, as illustrated in Fig. 1. An optical laser trap is used to facilitate and apply force in a defined direction on the exposed portion of the cell membrane *via* its receptors. Then, utilizing immunostaining for proteins of interest, *i.e.* vinculin in our case, the recruitment of protein is studied upon application of an external tensile load. In addition, the mechanical properties of the FA complex can be inferred from the measurement. The main advantages of the proposed method are controllability, physiological environment, introducing beads, ease of numerical simulations, local excitation with defined geometry, and most importantly the capability to directly image protein recruitment, which other techniques such as atomic force microscopy or micropipette aspiration may not offer.

Materials and methods

Microfluidic device design

A new microfluidic device was designed consisting of two separate channels into which either cells or beads could be introduced, multiple cell wells, and communicating or interconnecting narrow channels (Fig. 2). The interconnecting narrow channels connect the bead channel to each cell well in the cell channel. Beads are manipulated by an optical trap from the bead channel toward each single cell through these interconnecting channels. This microfluidic device provides a unique ability to position a single cell in a certain location. The concept is based on creating pressure gradients inside channels. The pressure gradient can be created by adding solution in either inlet ports of cell or bead

channels. This will then cause the flow of solution, due to gravitational driving force, in the direction of designated choice. For example, one may create pressure gradients in the cell channel from right to left, in the bead channel from left to right, and across interconnecting channels from up to down, as seen in Movie S0.† The microfluidic device was designed using AutoCAD (Autodesk, CA) with channel widths of 500 μm and 200 μm for cells and beads, respectively. Multiple seats (11 wells in this case) are located 250 μm apart over the 8 mm length of the cell channel. Cell seats measure 40 μm \times 30 μm and are identified numerically, as depicted in Fig. 2(b). The length of the interconnecting channels is 60 μm with a square cross section of 5 μm \times 5 μm at the junction between these channels and cell wells so that the exposed area of the cell after trapping in its well is 25 μm^2 . The height of all channels and features is 50 μm except the interconnecting channels with 5 μm height. Two separate inlets and outlets are used to create pressure gradients and to insert cells and beads into each channel.

Microfluidic device fabrication

The microfluidic device is fabricated in polydimethylsiloxane (PDMS) using master silicon wafers. Silicon wafers are made by photolithography using two different grades of SU-8 photoresist, SU-8 2005 and SU-8 2050 (MicroChem, MA), which can provide two distinct thicknesses of 5 μm and 50 μm at 2000 rpm and 3250 rpm spin speed, respectively. Since there are two different heights in our device, two separate negative photomasks are required. The negative photomasks are designed in AutoCAD and printed onto 100 μm thick polyester sheets (PageWorks, MA). Before any fabrication or SU-8 coating, the silicon wafers are cleaned and dehydrated on hot plate for 6 min at 160 $^{\circ}\text{C}$. Briefly, the fabrication process is to (i) spin coat with SU-8, (ii) soft bake on hot plate, (iii) expose to UV, (iv) post exposure bake on hot plate, (v) develop with PM Acetate, rinse with IPA (isopropanol) and dry with nitrogen N_2 . However, this process is repeated twice for the two separate photomasks as elaborated in Table 1. Precise alignment is required when each photomask is placed on the SU-8 coated wafers prior to UV exposure. The edge beads or

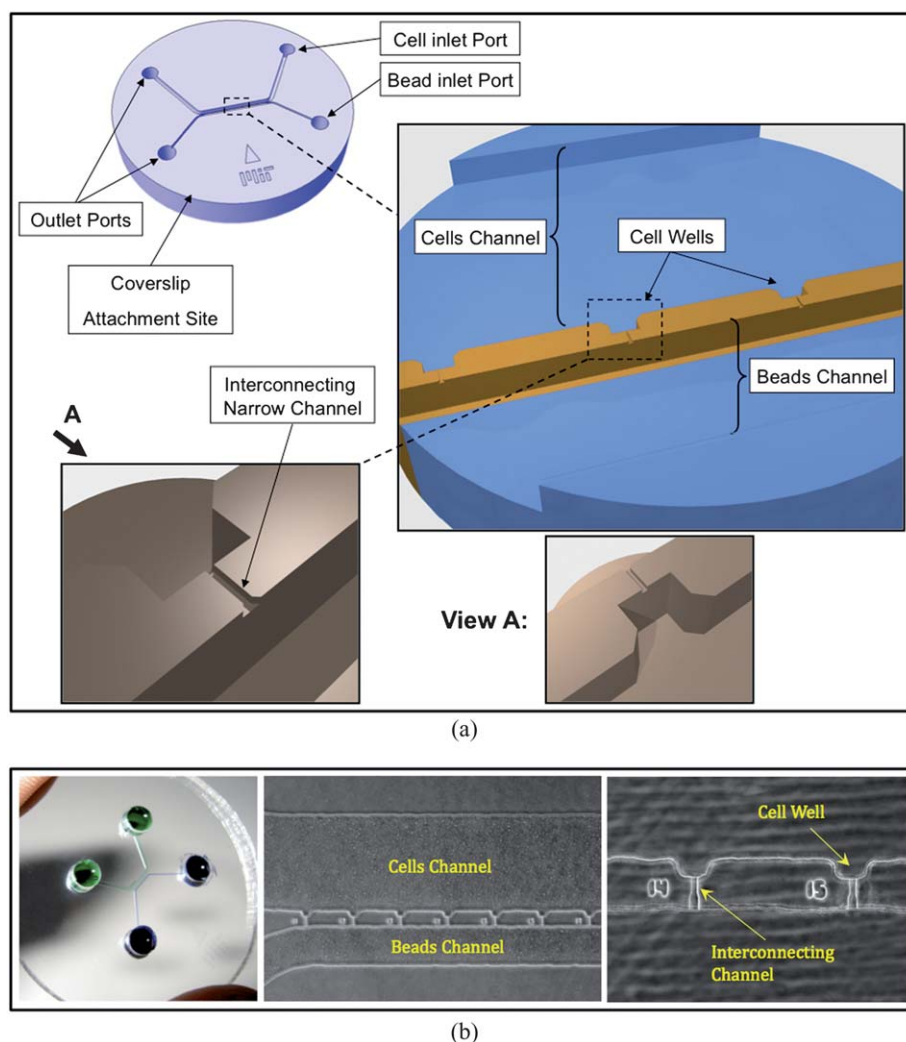


Fig. 2 (a) 3D-schematic representation of microfluidic device with upward patterned surface. A circular coverslip glass is attached on top, (b) Different resolutions of device and channels after fabrication. Channels are filled with food coloring for better visualization.

strings, if any, are removed from wafer to ensure close contact with photomasks.

Master wafers are used for PDMS replica molding.³⁰ PDMS prepolymers are prepared by mixing an elastomer-based precursor with a resin-based curing agent at a ratio of 10 : 1 (Silgard 184, Dow Chemical, MI). To remove air bubbles, the PDMS prepolymers is degassed in vacuum container for 20–30 min before casting on master silicon wafer, which plays as a mould. The PDMS is poured over the mould and is again degassed for 5–10 min to eliminate any remaining bubbles, then baked in oven (80 °C) for at least 4 h. The polymerized PDMS replica is peeled from the master wafer, each individual microfluidic device is trimmed (35 ± 2 mm diameter, 3 ± 1 mm

thickness), and inlets and outlets are punched out using a blunt-tip needle (Harris Uni-Core I.D. 3 mm). The surface of PDMS device is cleaned using adhesive tape to remove any residual dust. Both the fabricated PDMS device and glass coverslip (circular Ø35 × 0.2 mm, VWR International, PA) are sterilized at 120 °C for 20 min in a wet cycle followed by a dry cycle at 120 °C for 35 min with an autoclave (SR-24B; Consolidated Sterilizer Systems, MA). Finally, both the PDMS device and coverslip are plasma treated for 45 s with high power (29.6 W) using Plasma Cleaner (PDC-001, Harrick, CA), and permanently bonded to form a sealed microfluidic channel. The fabricated device, shown in Fig. 2(b), is utilized within 30 min after plasma treatment in order to facilitate filling by surface tension.

Table 1 The detailed process information of master wafer fabrication

Layers height	SU-8 grade	Spin speed	Soft bake	UV exposure	Post exposure bake	Develop time
5 µm	2005	2000 rpm	1 min @ 65 °C 2 min @ 95 °C	(2 × 20) s 110 mJ cm ⁻²	1 min @ 65 °C 3 min @ 95 °C	~2 min
50 µm	2050	3250 rpm	1 min @ 65 °C 7 min @ 95 °C	(17 × 3) s 160 mJ cm ⁻²	15 min @ 65 °C 6 min @ 95 °C	4–5 min

Cell culture protocol

Adult Human Dermal Microvascular Endothelial Cells (HMVEC-dAd; Lonza, MD) are used in all of our experiments. For cell culture, EGM2MV-Microvascular Endothelial Cell Growth Medium-2 (Lonza, MD) is used to support the growth and expansion of HMVEC cells. This cell culture medium consists of Lonza Basal Medium or DMEM (500 ml) mainly supplemented with FBS (25 ml); VEGF (0.5 ml); hEGF (0.5 ml); hydrocortisone (0.2 ml); GA-1000 (0.5 ml); hFGF-B (2.0 ml); R3-IGF-1 (0.5 ml); ascorbic acid (0.5 ml).

First, Filter-capped sterile flasks (T-12.5 cm²; VWR International, PA) are coated with collagen-I (BD Biosciences, MA) as follows. The collagen-I (1 ml; 50 μg ml⁻¹) is added to a sterile flask (T-12.5) and incubated for minimum 45 min at 37 °C. After the process of surface coating with collagen, the flask is rinsed three times with PBS. The cell culture media (3 ml) is warmed in a heat bath (37 °C) and added into each flask, ready for subsequent cell culture. Then, a cryopreserved vial of HMVEC (250 μl, 1 × 10⁶ cells ml⁻¹) is removed from the liquid nitrogen storage tank and is quickly thawed by placing the lower half of the vial in the water bath (37 °C) for 1 min. After thawing, cells are suspended in the vial gently by pipetting few times with micropipette. The cell suspension (250 μl) is pipetted into a 15 ml tube with 10 ml media. This tube spins in a centrifuge for 5 min at 1200 rpm. After centrifuge, supernatant is aspirated and fresh medium (200 μl) is added to the tube. To break the cell clumps, cells are resuspended gently by pipetting. The cell suspension is removed and split into four collagen-coated flasks (T-12.5) according to the Lonza recommendation of cell density (5000 cells cm⁻²). Then, the flasks are placed in a humidified incubator and their endothelial cell growth medium is changed every other day until cells reach to 80–85% confluent. For subculture, the cells are suspended using Trypsin-EDTA (0.05%, 1×, GibCo; invitrogen, CA), and the mix of cells and solutions (1 ml trypsin and 4 ml EGM-2MV) are decanted into 15 ml tube and centrifuge at 1200 rpm for 5 min. Similarly, cells are split over the collagen-coated flasks and expanded by endothelial cell growth media (EGM-2MV; Lonza, MD). Passage 7 cells are consistently used in all experiments. All cell culture procedures are handled inside a sterile hood, and cells are maintained in a humidified incubator at 5% CO₂ and 37 °C temperature control.

Experimental protocol

After microfluidic device preparation, devices are filled with sterile phosphate buffered saline (PBS) (1×, pH 7.4, GibCo; invitrogen, CA), while the channels are still hydrophilic. By introducing the solution into inlet ports, gravity drives a flow of solution from inlet to outlet. Aspiration from outlet ports completes the filling process. The whole process was repeated multiple times as necessary to ensure a proper filling. To facilitate cell adhesion, the cell channel surface is treated with 50 μg ml⁻¹ collagen type I (BD Biosciences, MA) and incubated for 1 h at 37 °C. Sterile Casein solution (10 mg ml⁻¹; Sigma-Aldrich, MO) is introduced to the bead channel for 15 min to eliminate undesirable bead attachment to the channel surfaces. Because of Proline peptide in Casein structure, coating the bead channel with Casein is very helpful in that regards. All channels are

washed with sterile PBS after each of these surface treatments. Subsequently, cell and bead inlet ports are each filled with 50 μl of endothelial cell growth medium (EGM-2MV; Lonza, MD). Devices are kept in a humidified incubator (5% CO₂ and 37 °C) for a minimum of 20 min before the insertion of endothelial cells.

Adult human dermal microvascular endothelial cells (HMVEC-dAd) are cultured in a flask about four days in advance and used upon reaching 80–85% confluence. The cells are suspended under the presence of Trypsin–EDTA (0.05%, 1×, GibCo; invitrogen, CA) for up to 4 min. The mix of cells and solutions (1 ml trypsin and 4 ml EGM-2MV) are decanted into 15 ml tube and centrifuge at 1200 rpm for 5 min. After Centrifuge, the supernatant is carefully aspirated and desire amount of fresh medium is added to the tube and pipetted up and down to create homogenous cell suspension. The cell suspension (15–20 μl) is added to the inlet port of the cell channel at density of 2 × 10⁶ cells ml⁻¹. The developed pressure gradient produces a flow that seats the cells into the cell wells.

Micro beads (2 μm polystyrene beads; Polysciences, PA) are coated with fibronectin type III (50 μg ml⁻¹; Sigma-Aldrich, MO) according to previously published articles.^{31–33} Carboxylated Polybeads are monodisperse polystyrene microspheres that contain surface carboxyl groups, allowing for covalent binding of fibronectin to the bead surface. In brief, beads were derivitized with biotin and subsequently coupled with avidin neutralite. Finally, beads were coupled with fibronectin-III and blocked with excess BSA; see^{31,33} for details. The solution concentration of fibronectin-coated beads is adjusted to the final concentration of 2 × 10⁴ beads μl⁻¹ by adding sterile cell culture water. Prior to insertion, the bead solution is sonicated for 15–20 min. The cells and beads are counted with Hemocytometer to maintain the constant density as needed in every experiment.

After insertion of cells (Fig. 3), the device is incubated for 5 min, and then mounted on a piezo-controlled stage (Polytech PI, Auburn, MA) associated with the optical laser system for mechanical stimulus. Beads are trapped singly by optical tweezers and are carried within the narrow connecting channels to the exposed portion of the cell membrane. Monotonic tensile force is locally applied to cells that are properly seated. Following force application, the cells are immediately fixed with 4% paraformaldehyde (PFA) and tagged with a fluorescent antibody for

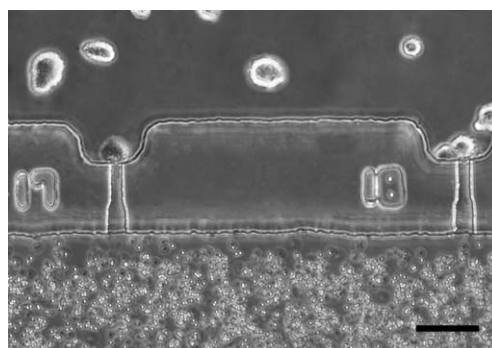


Fig. 3 Insertion of cells and beads separately into cell and bead channels. Cells are located properly on their wells, and beads are in position to be trapped and manipulated by optical tweezers. The pressure of cell channel is higher than bead channel not allowing any beads travel to the cell channel from the interconnecting channel. (Scale bar: 50 μm).

the proteins of interest and imaged by fluorescence microscopy. Note that microfluidic devices with seeded cells were not outside of the incubator for more than ~25 min before fixation.

Staining and fluorescence imaging

Immunofluorescence staining is performed to identify nucleus, vinculin and F-actin. Cells are fixed immediately following the optical trap experiment with 4% paraformaldehyde (Sigma-Aldrich, MO) for 30 min at room temperature. Then, the cell membrane is permeabilized with 0.1% Triton X-100 (Sigma-Aldrich, MO) for 15 min. After cells are fixed and permeabilized, they are incubated with Block Ace (Dainippon Pharmaceutical, Japan) for 1 h at room temperature. The primary antibody (monoclonal anti-vinculin antibody produced in mouse (1 : 200; Sigma-Aldrich, MO)) is introduced overnight at 4 °C after inhibiting non-specific binding sites with blocking solution. The secondary antibody (goat anti-mouse IgG (1 : 200; Sigma-Aldrich, MO) conjugated with AlexaFluor 488) is applied for 5 h in a dark chamber at room temperature. Finally, actin filaments and nuclei are stained with Rhodamine Phalloidin (1 : 40; Sigma-Aldrich, MO) and DAPI (1 : 1000; Sigma-Aldrich, MO), respectively. The mixture of Rhodamine Phalloidin and DAPI is introduced to the device for 3 h at room temperature. Between all staining steps, it is necessary to wash with three changes of PBS (1×, pH 7.4) for 45 min each. 15–25 min flow is followed by static conditions. Negative control is also conducted to assure that the vinculin protein is stained properly in the immunofluorescent process. This control has been accomplished by excluding the primary antibody sequence from the rest of staining procedure. Then, after fluorescent imaging, there was no green fluorescent anywhere in the samples suggesting that secondary antibody properly specifies only vinculin proteins.

After staining, all samples are examined using a fluorescence microscope (Nikon TE300, Japan) with appropriate filters. Fluorescent images are obtained using a phase-contrast microscope equipped with fluorescent filters *via* Openlab software (ver 5.5; Improvion, MA) and stored for further analysis. For time acquisition imaging, a time-lapse microscope (Nikon TE2000, Japan) is used with imaging software (NIS-Elements, ver 2.35). Images are processed using ImageJ software (NIH, <http://rsbweb.nih.gov/ij/>) and the variations of fluorescent intensity are analyzed across the cells using MATLAB (MathWorks, MA).

Optical laser tweezers

A custom-built optical trap is used to apply mechanical stimuli and obtain the mechanical response of a single endothelial cell to external force. Briefly, optical trapping is achieved by focusing a coherent laser (1064 nm) using a high numerical aperture objective (100×, 1.40 NA oil; Nikon, Japan); see^{34,35} for details. Ytterbium-doped fiber laser was emitting a 1064 nm wavelength laser beam (IPG Photonics, Oxford, MA). A secondary 975 nm laser in combination with a position sensitive device (PSD, Pacific Silicon, West Lake Village, CA) monitors a trapped bead at the back focal plane with resolution <1 nm.³⁶ The light collected by a condenser is filtered and focused into the PSD by lens with the focal length of 35 mm. The working distance of the condenser is 1.92 mm. To facilitate condenser connection and

position detection with position sensitive system, the microfluidic device is fabricated relatively thin (~3 mm thickness).

Once a single cell is located in a cell well, the optical tweezers captures a bead from the bead channel and its vertical position is adjusted ~2.5 μm above the coverslip, which is approximately at the center of the 5 μm × 5 μm narrow channel. Stiffness of the trapping laser and position of the bead are calibrated before each experiment by using a free bead in a buffer. The trapped bead is then manipulated to make contact with the cell before applying force. Bonds between a fibronectin-coated bead and the cell membrane are formed after about 5 s attachment. Tensile or pulling force is imposed to the cell membrane by moving the piezo-controlled stage with the trapping laser fixed. The applied force can be estimated by recording both stage and bead positions during experiments. Bead displacement (PSD) and stage position are recorded every ~30 ms to determine the applied force and resultant membrane deformation. Modeling the trap as a linear spring, applied force is calculated by multiplying the bead displacement from the center of the trap by the trap stiffness.

The piezo-controlled stage and the PSD detection system allow us to monitor their positions at the resolution of 1 nm. The optical tweezers are operated automatically by custom codes using LabView (National Instruments, Austin, TX), which facilitate to control experimental runs and acquire data. A microscope objective with 100× magnification is used for image acquisition, and images are acquired using a CCD camera (CCD-100, DATE-MTI, Michigan, IN).

Numerical simulations

Fluid flow induced in this microfluidic device is analyzed using the Finite Element Method (FEM). The microfluidic module of Comsol Multiphysics (ver 3.5, Comsol Inc., MA) is used for FEM analysis. Navier–Stokes equations describe flow in viscous fluids with momentum balances for each component of the momentum vector in all spatial dimensions.³⁷ An incompressible laminar flow is assumed with constant density and viscosity. The flow is driven inside the micro channels by hydrostatic pressure due to the gravity. No-slip boundary conditions are applied at all rigid surfaces, and the effect of surface tension is considered for free surfaces. The pressure at the bottom of each port is obtained by considering the effects of both hydrostatic pressure and surface tension. The surface tension causes a pressure drop (Δp) that can be calculated by:

$$\Delta p = \frac{4\gamma_{la}\cos(\theta)}{D} \quad (1)$$

where θ is the contact angle, D is the port diameter, and γ_{la} is the surface tension between liquid–air. Three-dimensional simulations were conducted to obtain the characteristics such as velocity profile, and the FEM results are extracted at the 2D plane of interest inside the device. The following physical properties are considered for FEM simulations: fluid density $\rho = 1000 \text{ kg m}^{-3}$, dynamic viscosity $\mu = 10^{-3} \text{ Pa}\cdot\text{s}$, surface tension $\gamma_{la} = 0.072 \text{ N m}^{-1}$ at 25 °C, and contact angle between liquid and PDMS $\theta = 102^\circ$.^{38,39}

The wall shear stress, in general, is given by $\tau_w = -\mu\partial U/\partial y$. In rectangular channels, the following equation states the flow rate:

$$Q = \frac{\tau_w w h^2}{6\mu} \quad (2)$$

where w and h are width and height of the channel, respectively. The flow rate (Q) can be defined as the product of cross-sectional area (A) and the fluid velocity (U). Therefore, by rearrangement of eqn (2), the shear stress (τ_w) can be obtained from:

$$\tau_w = \frac{6\mu U}{h} \quad (3)$$

Having the velocity profile from FEM simulations, the shear stress can be approximated by eqn (3), and apparently the maximum shear stress occurs where the velocity profile is maximum in the case of constant height.

Results and discussions

Cell solution is introduced in each device such that cells locate in their predefined wells. To optimize the process of cell placement in the microfluidic device shown in Fig. 3, fluid dynamics simulations were conducted with the use of 3D FEM. In this simulation, the no-slip condition is imposed along inner channel walls, and constant pressure is applied at the inlet and outlet ports. The driving force is mainly the hydrostatic pressure created by the height of liquid column at the inlet port. Pressure at the bottom of each port is determined by considering the effects of both hydrostatic pressure and surface tension. For example, adding 20 μl of cell solution, equivalent to 2.8 mm height inside the cylindrical inlet port, will create an approximate pressure of 47.5 Pa at the bottom of inlet port. This pressure is sufficient to carry the cells inside the micro channels.

Two filling scenarios have been described for inserting the endothelial cells into this microfluidic device. The first is to insert the cell solution into the inlet cylindrical port A while the pressure is in balance in all ports. As demonstrated in Fig. 4(a), the flow and pressure gradient will occur from right to left with the maximum flow velocity of 0.897 mm s^{-1} at the cell channel. This maximum velocity depends on the volume of cell solution (20 μl) inserted into the inlet port, causing a maximum shear stress of ~ 0.11 Pa on the channel wall. Although the steady-state equations of incompressible Navier–Stokes equations are considered in the simulations, the filling of a microfluidic device is a transient process that is considered here as quasi-steady. The experimental value of maximum velocity, measured from a time-lapse Movie S1,† is about 0.77 ± 0.1 mm s^{-1} , quite comparable to the FEM result. In the time-lapse movie, the total number of frames and the time between frames are assigned and known. To obtain velocity from the movie, an arbitrary particle is selected and tracked frame by frame along a certain distance, which is known from the device geometry. The velocity is then estimated by dividing the distance over the elapsed time. Unlike the cell channel, the flow is bidirectional in the bead channel with the maximum flow velocity of 11 $\mu\text{m s}^{-1}$. Further, the velocity profile is obtained over the arc-length (EF line) of interconnecting channels demonstrated in Fig. 4(b). The maximum velocity across the interconnecting channel happens in the first cell well, which is about 21 $\mu\text{m s}^{-1}$ in the narrow channel shown in Fig. 4(b). The pressure gradient across interconnecting channels is from up (cell channel) to down (bead channel) that causes a cell to flow into its well adjacent to 5 $\mu\text{m} \times 5 \mu\text{m}$ narrow channel.

Maximum pressure drops across the wells can also be determined from the simulations. The maximum pressure drop is ~ 27 Pa across the first well and incrementally decreases down to ~ 20 Pa across the last cell well. However, the velocity field across the interconnecting channels decreases about 25% from right to left, as shown in Fig. 4(c). This suggests that the chance of locating a cell in a well is higher at the upstream than the downstream end.

The second filling scenario is to inject the same volume of cell solution into both inlet and outlet ports (A and B) of cell channel. To analyze this situation, 3D finite element simulations are conducted by applying pressures corresponding to 10 μl cell solution in both cylindrical ports A and B. As demonstrated in Fig. 4(d), bidirectional flows occur in both cell and bead channels. The maximum velocities in the cell and bead channels are about 4 and 11 $\mu\text{m s}^{-1}$, respectively, with the maximum shear stress of ~ 0.5 mPa. Although the flow rate in the cell channel is much lower than in the previous case, the cells actually have a higher probability of seating in their wells. In this case, maximum velocity occurs in the interconnecting channels (1.75 mm s^{-1}) as illustrated in Fig. 4(e). The maximum experimental value, measured from a time-lapse movie, was 1.4 ± 0.5 mm s^{-1} . The velocity profile is shown over the arc-length (EF line) for the interconnecting channel in Fig. 4(f). In contrast to the previous filling case, the velocity profile for all interconnecting channels is nearly constant ($U_{\text{max}} = 1.75 \pm 0.025$ mm s^{-1}), as shown in Fig. 4(f). The pressure gradient across this channel is again from up (cell channel) to down (bead channel) with the maximum pressure drop of ~ 23.5 Pa.

To summarize the numerical simulation, two filling scenarios were used for this specific microfluidic device. In the first scenario, after cell solution (*e.g.* 20 μl) was inserted into the cylindrical port A, the liquid started flowing in channels according to the direction shown in Fig. 4(a). The steady-state situation for this scenario was simulated and the results were demonstrated in Fig. 4(b) and Fig 4(c). This simulation is actually a snap shot of the flow at the beginning of filling and over time, ports A and B will come to be in pressure equilibrium. Because of the geometry of the channels, ports A and B will eventually be in balance, and the problem reverts to the second scenario similar to the addition of ~ 10 μl solution into both cylindrical ports A and B. In the second scenario, the liquid will flow to balance the pressure between the port sets of (A and B) and (C and D), and consequently the direction of flow changes as shown in Fig. 4(d). The simulation was conducted for this case and the results for this snap shot were shown in Fig. 4(e) and Fig 4(f). In practice, the process of filling the cell channel and locating a cell within the wells will always follow a combination of the abovementioned scenarios. That is, one may insert the cell solution only in port A, but because of high flow rate in cell channel, ports A and B will eventually attain pressure equilibrium and the filling procedure reverts to the second scenario. With this process, ECs can be placed in their wells facing to the 5 $\mu\text{m} \times 5 \mu\text{m}$ interconnecting channels. Here, the plate-like surface of the cell membrane is exposed to the bead channel *via* each interconnecting channel.

After locating cells properly in their wells, fibronectin-coated beads are used to activate the $\alpha_v\beta_3$ integrins, although the choice of ligand depends on the nature of the experiment. A single bead is trapped and maneuvered from the bead channel toward the cell

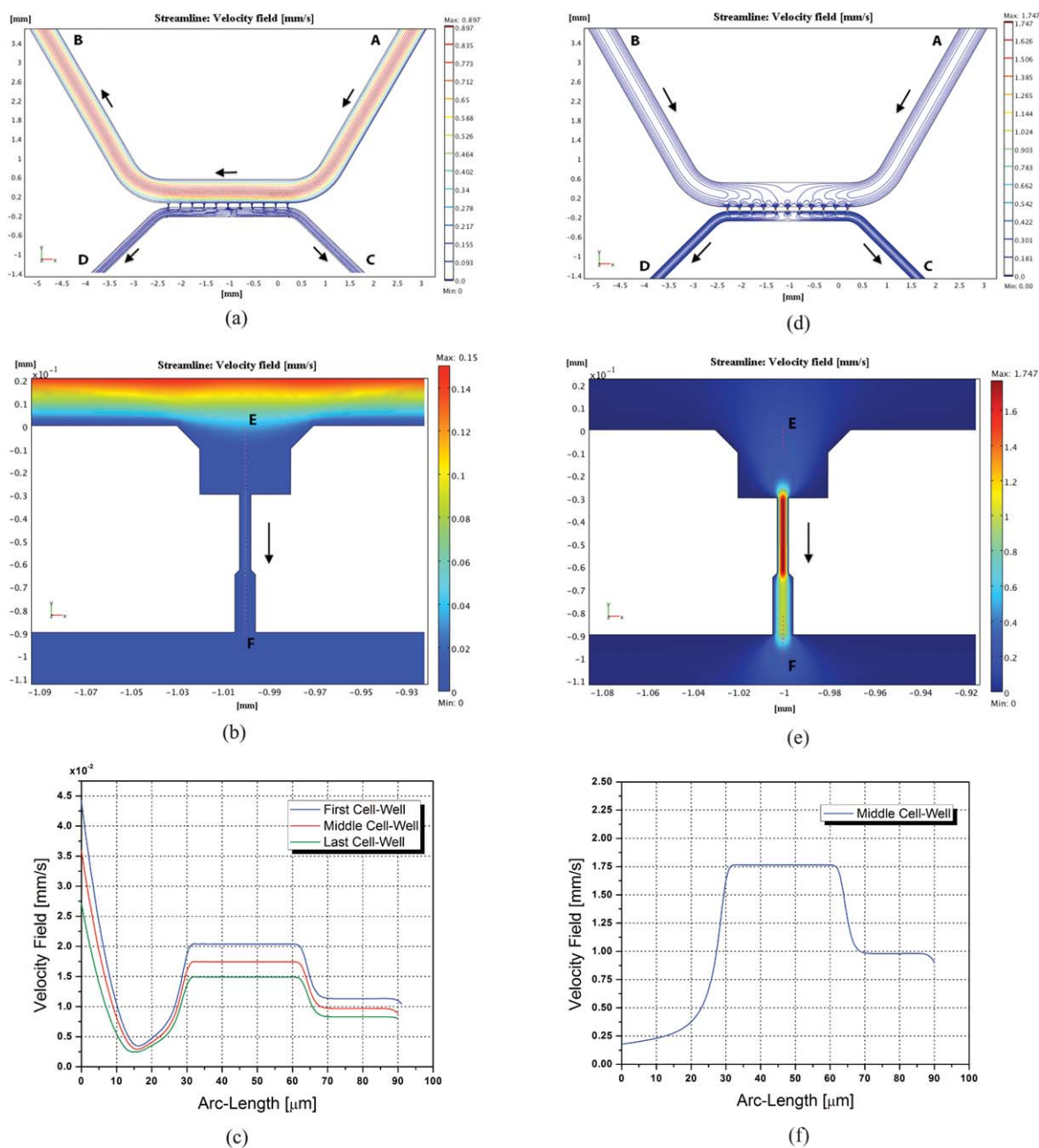


Fig. 4 (a) FEM results for velocity field in microfluidic channels when cell solution is inserted into only port A. (b) Velocity profile across the cell wells with maximum velocity of $15\text{--}21\ \mu\text{m s}^{-1}$ at $5\ \mu\text{m} \times 5\ \mu\text{m}$ narrow channels. The results are extracted in xy plane at the height of $2.5\ \mu\text{m}$ above coverslip. (c) Velocity variations along $90\ \mu\text{m}$ midline EF of three cell wells. (d) FEM results for velocity field in microfluidic channels when cell solution is inserted into both ports A and B. (e) Velocity profile across the cell wells with maximum velocity of $1.75\ \text{mm s}^{-1}$ at $5\ \mu\text{m} \times 5\ \mu\text{m}$ narrow channels. The results are extracted in xy plane at the height of $2.5\ \mu\text{m}$ above coverslip. (f) Velocity variations along $90\ \mu\text{m}$ midline EF of a cell well. This profile is almost identical among all cell wells, e.g. velocity across the narrowest section is $1.75 \pm 0.025\ \text{mm s}^{-1}$.

surface through an interconnecting narrow channel. Custom LabView codes are used to move the piezo-controlled stage and present the bead to the cell membrane in three steps (Movie S2†). First, by displacing the stage with a bead trapped by the optical tweezers, the bead approaches the cell membrane until it deviates from the center of the trap; next, the bead is held stationary against the membrane for 5 s to allow binding to occur between the bead and the membrane surface (arising integrin-fibronectin bindings). Finally, the stage is translated backward and as it is,

the force applied to the cell membrane *via* the trapped bead is monitored. Accordingly, tensile stress is conducted through integrins to the focal adhesion and cytoskeleton. Movie S2 demonstrates these steps for a single cell in each experiment.† Data are recorded at $\sim 33\ \text{Hz}$ sampling rate to compute the applied force and bead displacements.

The applied force is computed as the bead displacement relative to the center of the trapping beam multiplied by the stiffness of the trap.⁴⁰ Membrane deflection is computed as the difference

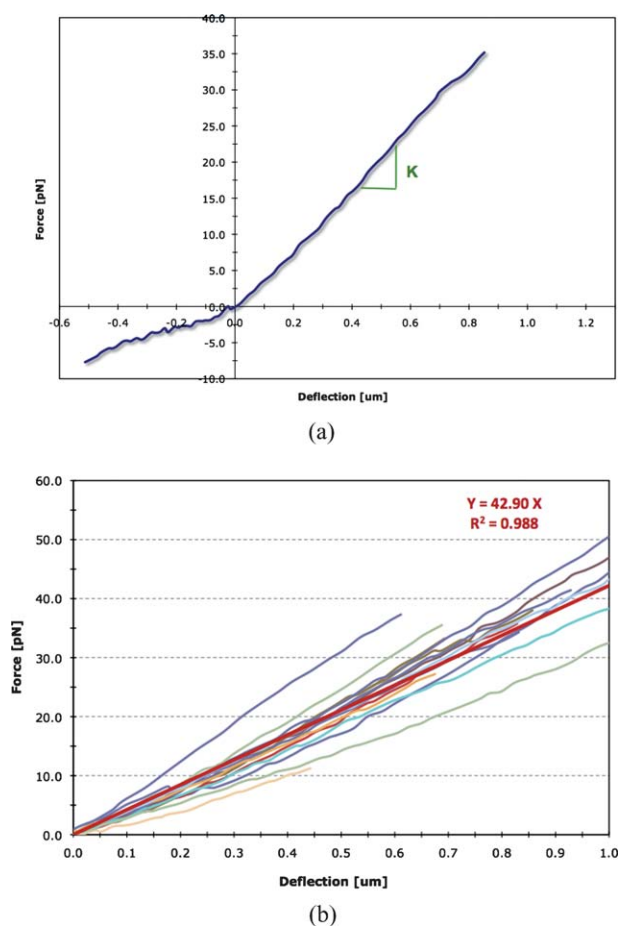


Fig. 5 (a) Applied force *versus* deflection curve of an isolated segment of cell membrane with typical trap stiffness of 0.11 pN nm^{-1} , (b) Resultant curve in linear region of applied tensile force *versus* deflection after regression analysis of 38 samples, e.g. 16 diverse lines are depicted besides the resultant red line.

between stage and bead displacements. A typical applied force *versus* membrane deflection trace is illustrated in Fig. 5(a). As indicated by the negative force, the cell is initially subjected to a compressive force. As the stage is retracted, the bead passes through the center of trap (zero force point) and the optical trap starts applying a tensile force to the square-like exposed region of the cell membrane. On further retraction, the cell is subjected to a progressively increasing tensile load until the bead escapes from the trap. The $2 \mu\text{m}$ bead escapes from the trap at a force of $42 \pm 8 \text{ pN}$ (mean \pm SD) and snaps back toward the cell, as seen in the Movie S2.† It should be noted that this level of force never broke the bonds between the bead and the cell membrane and beads always snapped back to the cell.

It appears that the nature of the cell-tethered bead is different depending on force direction, since the slope is lower in compression than in tension as plotted in Fig. 5(a). This suggests that the structural formation of focal adhesion proteins is promoted in tension and the cell membrane is more resistant to tensile stress. It should be noted, however, that the different index of refraction of the cell might interfere with the detection or tracking beams on compression when the trapping beam passes through the edge of the cell. For this reason, only tensile data are

reported here. However, this potential artifact is minimized by stopping the bead immediately after forming an initial contact. For each microfluidic device, a maximum of 2 to 3 individual cells could be studied with optical tweezers assay, due to concerns for cell viability. Thus, the data of 38 successful trials out of using many devices were considered for stiffness analysis, as indicated in Table 2 in the ESI.† Regression analysis of the tensile data ($n = 38$, the total number of individual cell samples) yields a plate-like membrane stiffness of $K = 42.9 \pm 6.4 \text{ pN } \mu\text{m}^{-1}$ (Fig. 5(b)) representing the combined stiffness of the FA assembly structure (such as fibronectin, integrin, vinculin, and talin linkage) as well as the cell membrane and cytoskeleton. These experimental data may be implemented in a numerical model to estimate the mechanical properties of subcellular structures in a molecular or continuum level model. By comparison, human red blood cells (RBCs), the linear elastic properties of the cytoskeleton-lipid bilayers composite have been reported as $22.1\text{--}29 \mu\text{N m}^{-1}$ for uniaxial tension.^{41,42} Because RBCs lack a full cytoskeleton and due to the FA structural proteins found in ECs, the value of stiffness found here ($42.9 \mu\text{N m}^{-1}$) is greater than that of a RBC, as expected.

It is instructive to consider these measurements in the context of a model in which it is assumed that all the stiffness is attributable to an elastic membrane constrained at the boundary of a $5 \mu\text{m}$ square exposed segment. Using Comsol Multiphysics, an FEM model is constructed according to the geometry and boundary conditions of the membrane segment ($5 \mu\text{m} \times 5 \mu\text{m}$, $t = 0.25 \mu\text{m}$). Reissner–Mindlin plate assumptions⁴³ are considered and the elastic modulus consistent with the observed deformations is calculated to be $4.01 \pm 0.51 \text{ kPa}$ assuming a thickness of 250 nm . This value of the elastic modulus falls within the range of other values reported in the literature⁴⁴ using a variety of measurement methods [micropipette aspiration, 114 Pa ,⁴⁵ atomic force microscopy, $1.5 \pm 0.76 \text{ kPa}$ to $5.6 \pm 3.5 \text{ kPa}$].

Immunofluorescent microscopy is conducted immediately after each tensile test. Cells are fixed and stained to identify the nucleus, F-actin, and vinculin as described in methods. Since beads are coated with fibronectin as an important ECM component, extracellular domain of the integrin proteins is activated after binding to fibronectin. This reaction transmits signals to the intracellular part of integrin triggering activation of talin and the formation of integrin-talin-actin complexes in the focal adhesion. At this point, the current hypothesis is that upon application of tension on this structure, cryptic binding sites of talin may be exposed and vinculin proteins bind and recruit to talin. Several groups have attempted to investigate this hypothesis computationally^{22,24} or experimentally.²⁶ However, our method is unique in the sense of having a pure tensile force, defined boundary condition, computational benefit, traceability, imaging ability, and activation control of different transmembrane proteins, in addition to all advantages of controlled microfluidic environment. Moreover, in this method, a laser beam approaches from the side rather than directly illuminating the cell, which may impair detection (due to the different index of refraction) and damage the cells (due to local heat generation). In an earlier study,²⁶ force is applied parallel to the membrane surface creating, from the molecular perspective, complex shear and tensile forces beneath the bead. However, in the current experiment, a perpendicular force is applied to the membrane,

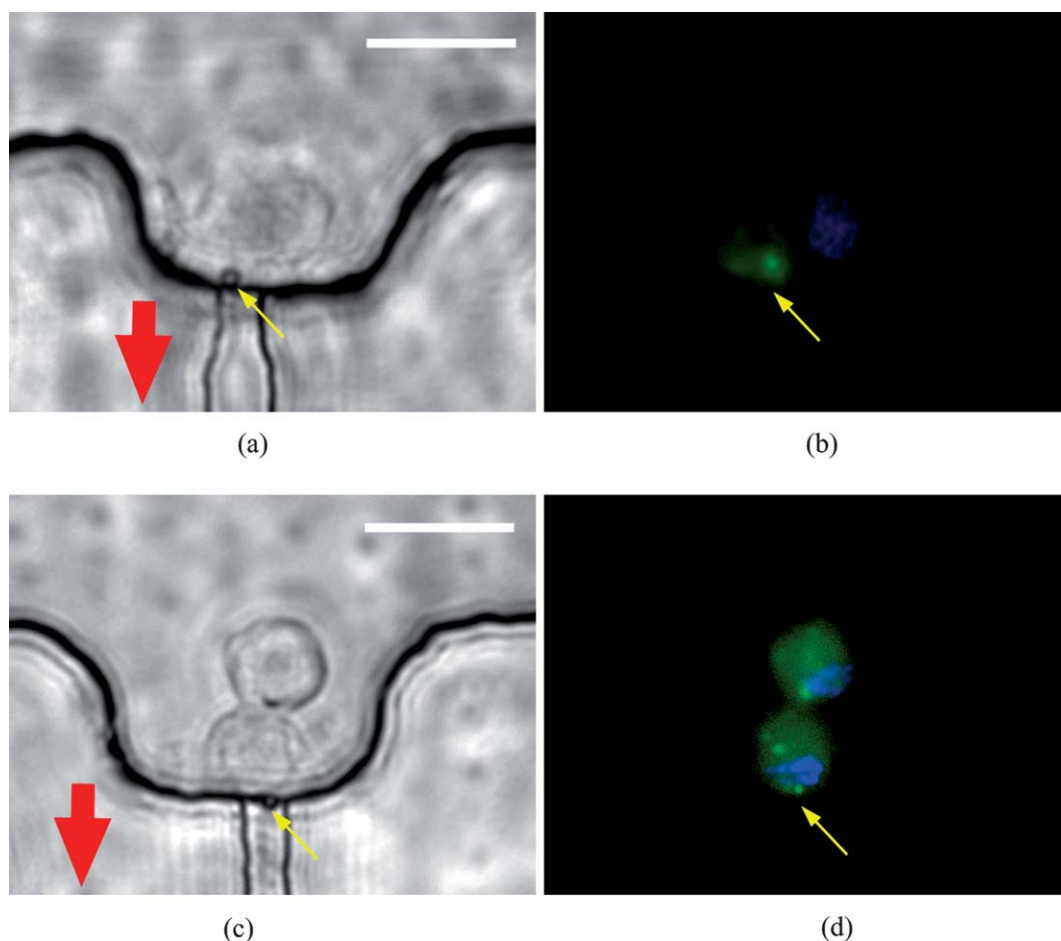


Fig. 6 (a) and (c) Phase contrast images of cells located in their wells with an attached bead to their membrane surface. (b) and (d) Fluorescent images of vinculin distribution (green) and nucleus (blue) after the application of tension. Yellow arrows refer to a bead location in both corresponding phase and fluorescent images; all scale bars: 20 μm .

which causes tensile stress in all transmembrane receptors, *i.e.* integrins. This method may be considered as a standard or generalized technique to apply a locally tensile stress and to identify the proteins of interest affiliated in mechanotransduction for various cell lines.

Proceeding with fixation and staining, cells locally subjected to tension are of interest, for which fluorescent images are obtained. Two typical brightfield and fluorescent images are illustrated in Fig. 6 for cells that are subjected to tensile test *via* fibronectin-coated beads using the optical trap. In each experiment, vinculin recruitment is observed in the vicinity of the attached bead. In Fig. 6(a) and (c), the direction of pulling and the attached bead are shown by red and yellow arrows, respectively.

In Fig. 6(b) and (d), regions of vinculin recruitment can be observed with respect to the yellow arrows. It is important to highlight that vinculin appears to be recruited above the bead as an elliptical cloud, in contrast to its recruitment on cells after spreading that is similar to longitudinal short strands accumulated on the membrane edge.⁴⁷ The center-to-center distance between this protein cloud and the bead is about $2.1 \pm 0.5 \mu\text{m}$ measured for 31 individual cells, see Table 2 in the ESI.† The reason for this apparent displacement is not immediately clear, but was a consistent finding. However, a possible reason for the vinculin cloud could be a tensile stress that actually propagates in

an elliptical shape inside the cytoskeleton until it damps. Therefore, many proteins may be subjected to tension including talin connected to β -integrin adjacent to the membrane. Because

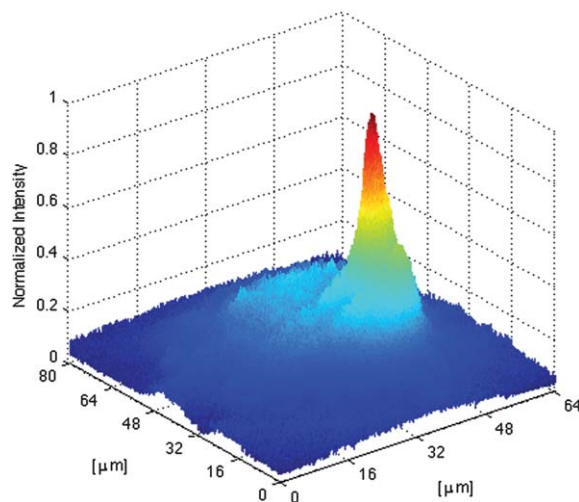


Fig. 7 Normalized intensity of vinculin recruitment over a cell area after application of tensile force. Transition between light to dark blue is cell border and highest peak is intensity adjacent to a bead.

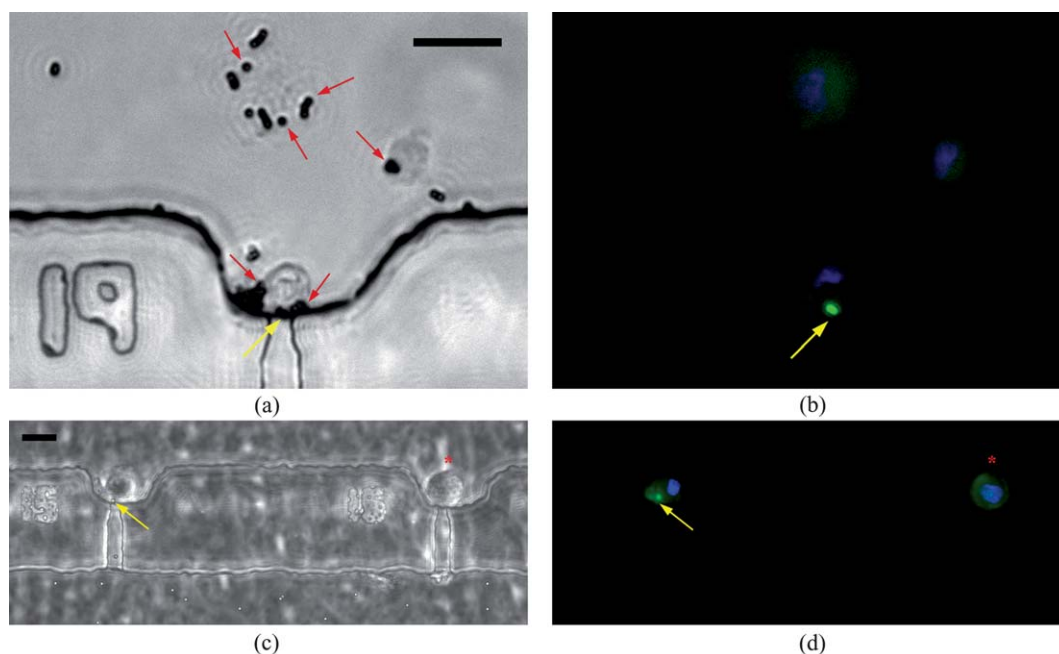


Fig. 8 (a) and (b) Phase contrast and fluorescent image of a sample with beads (red arrow) on both cell and bead channels while force applied on couple of them (yellow arrow); scale bar: 20 μm . (c) and (d) Phase contrast and fluorescent image of a sample with two cells located in their seats. The left cell is excited with the functionalized bead (yellow arrow), while the right cell (*) just sits in its well without any bead attachment and manipulation; scale bar: 30 μm .

of tension, the talin rod domain will be activated and the vinculin head domain binds to talin.^{23,25} Nevertheless, vinculin possesses many binding partners other than talin;¹⁶ for instance, the vinculin is also known to bind to F-actin^{48,49} or α -actinin.^{50,51} The protein cluster above the bead may suggest that from a molecular point of view, not only tension promotes vinculin recruitments to talin, but it may also induce binding of vinculin to other protein partners inside the cytoskeleton over the propagated tension region.

Intensity analyses were performed for images to assure of location and protein recruitment in comparison with other parts of a cell, as shown in Fig. 7. A comparison between cells with and without tensile stress shows that cells under tensile stress have a peak in intensity above the bead, while the cells without any external stress possess an almost uniform distribution of vinculin over the cell area. Occasionally, a few more bright regions other than the bright region adjacent to the bead were observed. The source of vinculin recruitments in those bright regions is the creation of local tensile forces in those regions. For example, the onset of cell attachment or cell–cell adhesion may exert internal tensile forces causing vinculin recruitments in the contact region. In general, cells always attach by their transmembrane proteins, *e.g.* integrins, cadherins and so on, to the substrate or other adjacent cells. Therefore, those transmembrane proteins can only convey a mechanical force from outside to the cytoskeleton causing vinculin recruitment.

As a control, beads were also tethered to the cell without the application of force. In Fig. 8(a), although the functionalized beads are deliberately introduced into both channels, only two beads are trapped and pulled. In Fig. 8(b), the fluorescent image shows the bright spot above only those beads that are pulled by optical trap. Other beads in contact with the cell membrane but

not under force exhibit less vinculin recruitment. In 31 out of 38 cells under tension, vinculin recruitment was observed adjacent to the bead. This suggests that there is a clear connection coupling vinculin activation to the applied tensile force. Fig. 8(c) and (d) show two cells both of which sit properly in their wells. The one on the left under force recruits vinculin whereas the one on the right (*) without force does not. Without application of any force, the same phenomena have been observed for 15 cells out of 15. This suggests that fibronectin binding to integrins is not sufficient by itself to induce vinculin clustering; tensile force is also necessary.

Summary

In this research, a new methodology is introduced to apply mechanical tensile force to membrane receptors and focal adhesion complexes. The current experimental setup provides a means to test and understand the mechanism by which focal adhesion proteins are activated upon application of external force. Combination of a well-designed microfluidic device with optical tweezers provides the possibility of applying mechanical stimuli horizontally and locally on the defined region of the cell membrane. In comparison with other techniques, this method possesses many advantages such as defined boundary conditions, simultaneous force and fluorescence imaging, and the capability to study the effect of many ECM proteins other than fibronectin. Using fibronectin-coated beads facilitates ECM-integrin-talin-actin linkages. The current study provides solid evidence that mechanical tension is required for the initiation and stabilization of these structures, and vinculin is recruited to focal adhesions upon transduction of tensile load. Although vinculin recruitment is emphasized in current research, this framework could be

considered as a systematic method to recognize and identify mechanosensitive proteins that are affiliated with mechanotransduction in FA domains. The mechanical properties of this FA complex are linearly elastic at the early stage of formation. It is important to emphasize that the present microfluidic device may have many capabilities and applications. As a continuation of this work, using a similar microfluidic device, one may study the effects of specific chemical media locally on a cell while those media are introduced into the bead channel instead of beads. Furthermore, the adapted version of this microfluidic device may be used in disease diagnosis by tracing protein recruitment and comparing pulling data between healthy and unhealthy cells.

Acknowledgements

The financial supports from Natural Sciences and Engineering Research Council of Canada (NSERC) and SMART center are greatly appreciated. Authors would like to thank Dr Sid Chung, Dr Ryo Sudo, and Dr Chandra Kothapalli for their contributions and useful discussions along the path of this research.

References

- 1 M. Vicente-Manzanares, C. K. Choi and A. R. Horwitz, *J. Cell Sci.*, 2009, **122**, 199–206.
- 2 J. Liu, X. He, S. A. Corbett, S. F. Lowry, A. M. Graham, R. Fassler and S. Li, *J. Cell Sci.*, 2009, **122**, 233–242.
- 3 D. S. Harburger and D. A. Calderwood, *J. Cell Sci.*, 2009, **122**, 159–163.
- 4 C. H. Streuli, *J. Cell Sci.*, 2009, **122**, 171–177.
- 5 E. Puklin-Faucher and M. P. Sheetz, *J. Cell Sci.*, 2009, **122**, 179–186.
- 6 D. R. Critchley, *Curr. Opin. Cell Biol.*, 2000, **12**, 133–139.
- 7 D. R. Critchley and A. R. Gingras, *J. Cell Sci.*, 2008, **121**, 1345–1347.
- 8 D. A. Calderwood, *J. Cell Sci.*, 2004, **117**, 657–666.
- 9 A. R. Gingras, N. Bate, B. T. Goult, L. Hazelwood, I. Canestrelli, J. G. Grossmann, H. Liu, N. S. Putz, G. C. Roberts, N. Volkmann, D. Hanein, I. L. Barsukov and D. R. Critchley, *EMBO J.*, 2008, **27**, 458–469.
- 10 A. R. Gingras, W. H. Ziegler, A. A. Bobkov, M. G. Joyce, D. Fasci, M. Himmel, S. Rothmund, A. Ritter, J. G. Grossmann, B. Patel, N. Bate, B. T. Goult, J. Emsley, I. L. Barsukov, G. C. Roberts, R. C. Liddington, M. H. Ginsberg and D. R. Critchley, *J. Biol. Chem.*, 2009, **284**, 8866–8876.
- 11 B. Xing, A. Jedsadayanmata and S. C. Lam, *J. Biol. Chem.*, 2001, **276**, 44373–44378.
- 12 L. Hemmings, D. J. Rees, V. Ohanian, S. J. Bolton, A. P. Gilmore, B. Patel, H. Priddle, J. E. Trevithick, R. O. Hynes and D. R. Critchley, *J. Cell Sci.*, 1996, **109**(Pt 11), 2715–2726.
- 13 A. R. Gingras, K. P. Vogel, H. J. Steinhoff, W. H. Ziegler, B. Patel, J. Emsley, D. R. Critchley, G. C. Roberts and I. L. Barsukov, *Biochemistry*, 2006, **45**, 1805–1817.
- 14 C. Bakolitsa, J. M. de Pereda, C. R. Bagshaw, D. R. Critchley and R. C. Liddington, *Cell*, 1999, **99**, 603–613.
- 15 J. D. Humphries, P. Wang, C. Streuli, B. Geiger, M. J. Humphries and C. Ballestrem, *J. Cell Biol.*, 2007, **179**, 1043–1057.
- 16 W. H. Ziegler, R. C. Liddington and D. R. Critchley, *Trends Cell Biol.*, 2006, **16**, 453–460.
- 17 A. P. Gilmore, P. Jackson, G. T. Waites and D. R. Critchley, *J. Cell Sci.*, 1992, **103**(Pt 3), 719–731.
- 18 A. R. Menkel, M. Kroemker, P. Bubeck, M. Ronsiek, G. Nikolai and B. M. Jockusch, *J. Cell Biol.*, 1994, **126**, 1231–1240.
- 19 M. Kim, C. V. Carman, W. Yang, A. Salas and T. A. Springer, *J. Cell Biol.*, 2004, **167**, 1241–1253.
- 20 R. O. Hynes, *Cell*, 2002, **110**, 673–687.
- 21 V. Vogel and M. Sheetz, *Nat. Rev. Mol. Cell Biol.*, 2006, **7**, 265–275.
- 22 S. E. Lee, R. D. Kamm and M. R. Mofrad, *J. Biomech.*, 2007, **40**, 2096–2106.
- 23 S. E. Lee, S. Chunsriviro, R. D. Kamm and M. R. Mofrad, *Biophys. J.*, 2008, **95**, 2027–2036.
- 24 V. P. Hytonen and V. Vogel, *PLoS Comput. Biol.*, 2008, **4**, e24.
- 25 A. del Rio, R. Perez-Jimenez, R. Liu, P. Roca-Cusachs, J. M. Fernandez and M. P. Sheetz, *Science*, 2009, **323**, 638–641.
- 26 C. G. Galbraith, K. M. Yamada and M. P. Sheetz, *J. Cell Biol.*, 2002, **159**, 695–705.
- 27 G. Giannone, G. Jiang, D. H. Sutton, D. R. Critchley and M. P. Sheetz, *J. Cell Biol.*, 2003, **163**, 409–419.
- 28 G. Jiang, G. Giannone, D. R. Critchley, E. Fukumoto and M. P. Sheetz, *Nature*, 2003, **424**, 334–337.
- 29 S. T. Kim, K. Takeuchi, Z. Y. Sun, M. Touma, C. E. Castro, A. Fahmy, M. J. Lang, G. Wagner and E. L. Reinherz, *J. Biol. Chem.*, 2009, **284**, 31028–31037.
- 30 J. C. McDonald, D. C. Duffy, J. R. Anderson, D. T. Chiu, H. Wu, O. J. Schueller and G. M. Whitesides, *Electrophoresis*, 2000, **21**, 27–40.
- 31 D. P. Felsenfeld, P. L. Schwartzberg, A. Venegas, R. Tse and M. P. Sheetz, *Nat. Cell Biol.*, 1999, **1**, 200–206.
- 32 G. von Wichert, B. Haimovich, G. S. Feng and M. P. Sheetz, *EMBO J.*, 2003, **22**, 5023–5035.
- 33 G. von Wichert, G. Jiang, A. Kostic, K. De Vos, J. Sap and M. P. Sheetz, *J. Cell Biol.*, 2003, **161**, 143–153.
- 34 R. R. Brau, P. B. Tarsa, J. M. Ferrer, P. Lee and M. J. Lang, *Biophys. J.*, 2006, **91**, 1069–1077.
- 35 M. J. Lang and S. M. Block, *Am. J. Phys.*, 2003, **71**, 201–215.
- 36 F. Gittes and C. F. Schmidt, *Opt. Lett.*, 1998, **23**, 7–9.
- 37 F. M. White, *Fluid mechanics*, McGraw-Hill, Boston, 2003.
- 38 M. J. Owen, *J. Appl. Polym. Sci.*, 1988, **35**, 895–901.
- 39 X. B. Deng, R. Luo, H. L. Chen, B. L. Liu, Y. J. Feng and Y. H. Sun, *Colloid Polym. Sci.*, 2007, **285**, 923–930.
- 40 K. C. Neuman and S. M. Block, *Rev. Sci. Instrum.*, 2004, **75**, 2787–2809.
- 41 J. Li, M. Dao, C. T. Lim and S. Suresh, *Biophys. J.*, 2005, **88**, 3707–3719.
- 42 J. Li, G. Lykotraftitis, M. Dao and S. Suresh, *Proc. Natl. Acad. Sci. U. S. A.*, 2007, **104**, 4937–4942.
- 43 E. Reissner, *Appl. Mech. Rev.*, 1985, **38**, 1453–1464.
- 44 P. A. Janmey and C. A. McCulloch, *Annu. Rev. Biomed. Eng.*, 2007, **9**, 1–34.
- 45 M. Sato, D. P. Theret, L. T. Wheeler, N. Ohshima and R. M. Nerem, *J. Biomech. Eng.*, 1990, **112**, 263–268.
- 46 K. D. Costa, A. J. Sim and F. C. Yin, *J. Biomech. Eng.*, 2006, **128**, 176–184.
- 47 B. J. Dubin-Thaler, J. M. Hofman, Y. Cai, H. Xenias, I. Spielman, A. V. Shneidman, L. A. David, H. G. Dobreiner, C. H. Wiggins and M. P. Sheetz, *PLoS One*, 2008, **3**, e3735.
- 48 S. Huttelmaier, P. Bubeck, M. Rudiger and B. M. Jockusch, *Eur. J. Biochem.*, 1997, **247**, 1136–1142.
- 49 R. P. Johnson and S. W. Craig, *J. Biol. Chem.*, 2000, **275**, 95–105.
- 50 P. R. Bois, B. P. O'Hara, D. Nietlispach, J. Kirkpatrick and T. Izard, *J. Biol. Chem.*, 2006, **281**, 7228–7236.
- 51 D. F. Kelly, D. W. Taylor, C. Bakolitsa, A. A. Bobkov, L. Bankston, R. C. Liddington and K. A. Taylor, *J. Mol. Biol.*, 2006, **357**, 562–573.